Turkish Journal of Electrical Engineering & Computer Sciences

http://journals.tubitak.gov.tr/elektrik/

Research Article

Turk J Elec Eng & Comp Sci
(2020) 28: 3068 – 3078

doi:10.3906/elk-1903-103

Performance optimisation of a sensing chamber using fluid dynamics simulation for electronic nose applications

Punjan DOHARE[1,2,*], **Sudeshna BAGCHI**[1,2], **Amol P BHONDEKAR**[1,2]
[1]CSIR-Central Scientific Instruments Organisation, Chandigarh, India
[2]Academy of Scientific and Innovative Research, New Delhi, India

Received: 18.03.2019 • **Accepted/Published Online:** 16.10.2019 • **Final Version:** 25.09.2020

Abstract: The sensor chamber plays a significant role in order to improve the performance of an electronic nose in terms of stability, repeatability, reproducibility, and sensitivity. Fluid dynamics simulations of six different configurations of 3D sensing chambers are presented to facilitate the efficient design of an electronic nose system comprising 64 sensor arrays. Numerical simulations were carried out to investigate the gas (zero air) flow behaviour inside these chambers under steady-state conditions for velocities ranging from 0.1 to 2 m/s using ANSYS software. Design optimisation was performed in terms of area coverage, velocity, and mass fraction. The results show that the area coverage and mass fraction distribution increase with flow velocity. The sensor chambers achieved more than 70% flow coverage over the sensors at a velocity beyond 0.7 m/s. In further chamber designs, four baffles were introduced at different positions in a two inlet and one outlet chamber model to enhance the performance of the chamber. The effect of baffle positions in the flow distribution was investigated through numerical simulations. Chamber designs with the introduction of baffles achieved a maximum mass fraction. Thus, the insertion of baffles improved the area coverage and mass fraction. In addition, to show the real-time applicability further simulations were performed in the optimised sensor chamber.

Key words: Electronic nose, computational fluid dynamics, sensor chamber, baffle, numerical modelling

1. Introduction

The electronic nose was first conceived by Dodd and Persuad in 1982 with the aim of mimicking the biological system of human olfaction using pattern technology. Since then it has attracted widespread application in numerous fields including food quality and safety assessment [1], medical diagnostics [2, 3], environmental monitoring [4], explosive detection [5], etc.

An electronic nose generally consists of a odour delivery system, a detection system consisting of a sensor array, and computer system that learns, classifies, and identifies the electronic data for different aromas using pattern recognition. Numerous research works have focused on performance enhancement of the electronic nose through material and structural optimisation of the sensor array. Various novel material composites such as conducting polymers and carbon nanostructures have been explored as resistive [6], metal oxide semiconductor [7], piezoelectric [8], electrochemical [9], and optical gas sensors [10]. Although different performance parameters of the sensors were improved by tailoring the sensor materials, it is necessary to optimise the design of the sensor system for real-time applications. In particular, the sensor chamber needs to be efficiently designed for effective exposure of the sensors to vapours/gases with different analyte concentrations. The volume and structure of the

*Correspondence: punjan.nitk@gmail.com

chamber have to be designed such that the flow is homogeneously and evenly distributed over all the sensors. All sensors should be exposed to the same odour concentration.

There are very few published reports on the design and development of sensor chambers using fluid dynamics simulation [11–13]. Scott et al. [13] performed fluid dynamics simulation in a 2D model that was discretised by finite elements to optimise the position of quartz crystal microbalance (QCM) sensors in the chamber design for the volatile detection system. It was observed that sensors placed at 0° to the flow direction showed even flow distribution with no recirculation zone as compared to sensors placed at 90°. In the optimised sensor chamber with baffles, when sensors were at 0° to the flow direction with baffles the flow distribution was even over the sensors with no recirculation zone. Viccione et al. [14] used a three-dimensional computational fluid dynamics approach for four different geometries of a diffuser, which was discretised with finite volumes in order to improve the steady-state conditions in minimum time and ensure adequate contact time with the sensor surface.

However, further investigations are required to explore the effect of chamber design on sensor performance. Therefore, in the present study, a fluid dynamics simulation was carried out to analyse the performance of a sensor chamber for an electronic nose and attain the data to achieve the optimal chamber design. A simulation was carried out with three different three-dimensional models of the sensor chamber, which includes simple cuboidal configurations with single and multiple inlets/outlet. Furthermore, three chamber models were designed with the introduction of four baffles in the optimised cuboidal design.

2. Methodology

2.1. Sensor chamber designs

An 8×8 sensor array of 64 sensor element has been designed. The sensor elements have been placed at centre-to-centre distance of 5 mm. The sensor positions are organised in eight rows and eight columns in the inner face of the chamber bottom.

Six different three-dimensional sensor chamber designs are used to analyse the airflow dynamics with respect to the sensor element positions shown in Figures 1 and 2.

Chambers 1, 2, and 3 are simple cuboids with dimensions $52 \times 52 \times 10$ mm as shown in Figure 1. In further designs, initially, four baffles are introduced at random positions. The purpose is to ensure homogeneous flow over the sensors and to minimise swirling and recirculating zones. Simulations are carried out to select the optimised baffle positions. Initially, two baffles are placed at 0° and 90° with respect to the inlet and outlet in order to evenly distribute the flow and minimise the velocity gradient. In the subsequent step, the positions of these baffles are shifted to obtain the three best chamber designs. Furthermore, Figure 2 shows chambers 4–6 with four baffles having a length, width, and height of 10, 2, and 5 mm, respectively, to improve the airflow distribution inside the sensor chamber.

2.2. Numerical modelling

Six different three-dimensional models of sensor chambers were created using Solidworks CAD software. The sensor chamber models were discretised into unstructured tetrahedral mesh elements. Steady-state simulations are performed for the flow velocity ranging between 0.1 to 2 m/s using the software FLUENT. Flow velocity between 0.1 to 2 m/s was considered laminar flow. The Reynolds number at the chamber inlet is obtained in the range between 17 and 342. In the simulation, the fluid is zero air consisting of 78% (w/w) nitrogen and 21% (w/w) oxygen. FLUENT is used to predict the airflow through solutions, the conservation equation of mass

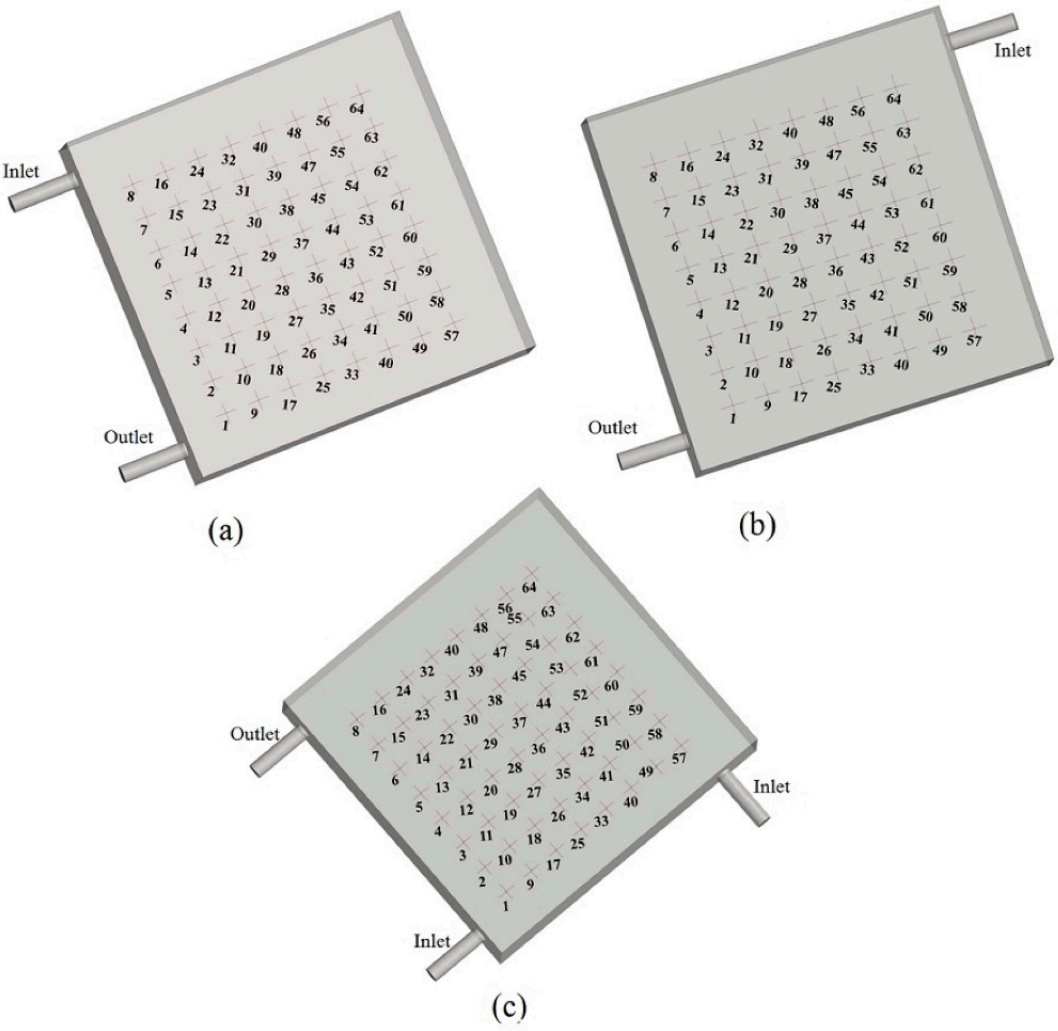

Figure 1. Three configurations of simple cuboids with different inlet and outlet positions: (a) sensor chamber 1 with inlet and outlet on the same axis; (b) sensor chamber 2 with inlet and outlet diagonally placed; (c) sensor chamber 3 with two inlets and one outlet.

(the continuity equation),

$$\frac{\partial \rho}{\partial t} = 0 \tag{1}$$

and Navier–Stokes equation expressed as

$$\rho \frac{DV}{Dt} = -\nabla P + \mu \nabla^2 V + \rho g, \tag{2}$$

where V is the velocity, P is pressure, ρ is the mass density of air, and μ is the dynamic viscosity coefficient. The second order upwind scheme was used to approximate the momentum equation. The pressure and velocity coupling were realised through the semiimplicit method for pressure-linked equation (SIMPLE) algorithm. The boundary conditions were as follows: (i) the sensor chamber walls were assumed to be rigid; (ii) no-slip boundary

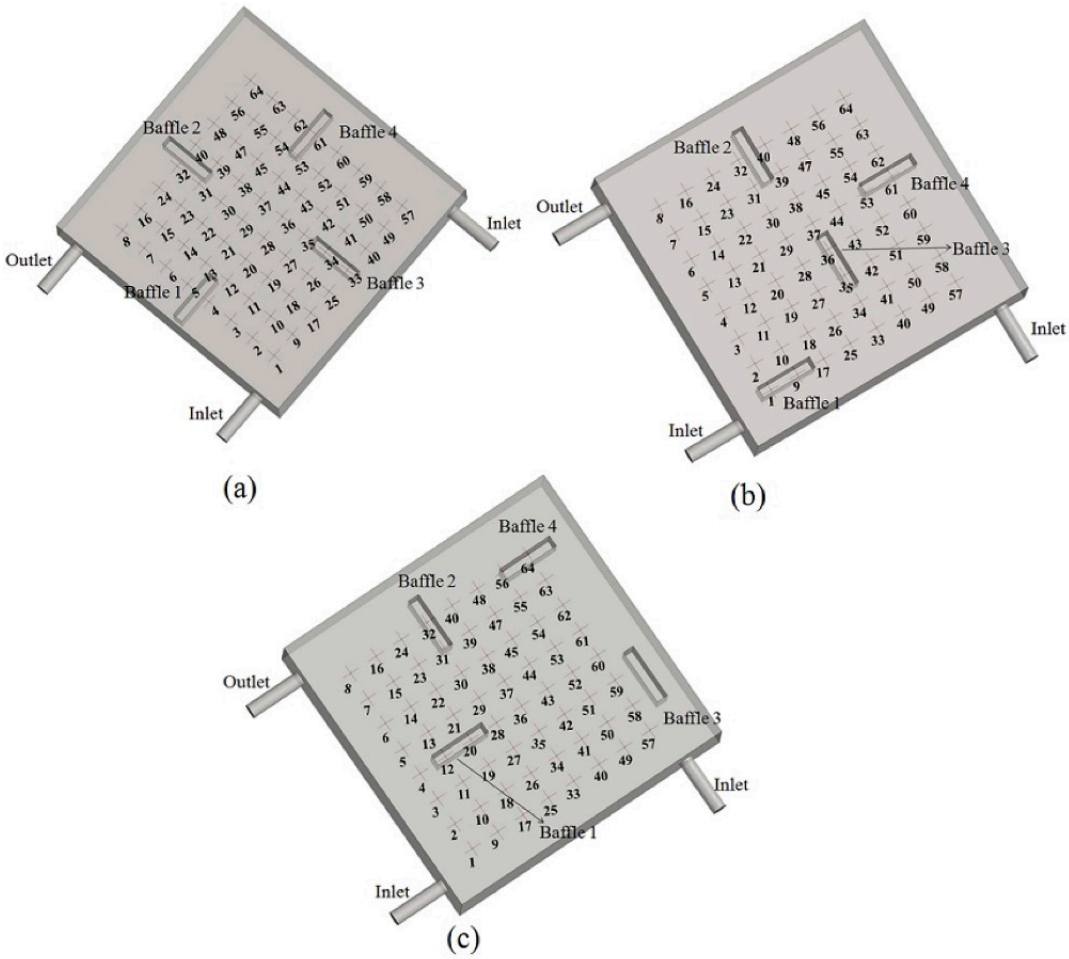

Figure 2. Sensor chambers 4, 5, and 6 containing two inlets and one outlet with four baffles at a different location (a), (b), and (c).

condition was defined at the chamber walls; (iii) zero pressure value was taken at the inlet and outlet of the sensor chamber. Density and dynamic viscosity of the zero air were 1.225 kg/m^3 and 1.7894×10^{-5} kg/m-s, respectively. The convergence of the solution was set to 0.001 for residual values of governing and transport equations.

3. Results and discussion

Simulations are carried out to analyse the fluid behaviour inside the sensor chamber using six three-dimensional models. The results are presented to observe the effects of flow velocity, position and number of inlets or outlets, baffles' positions and dimensions, area coverage in terms of percentage, and mass fraction.

3.1. Effect of position and number of inlets/outlet on flow distribution

The flow distribution results obtained from computational analysis of the chambers are represented in two-dimensional images displaying the velocity contours over the sensors. Velocity contours for sensor chamber 1 are shown in Figures 3a and 3b for flow velocities of 0.2 and 1.9 m/s, respectively. It is observed that for a

flow velocity of 0.2 m/s, the majority of the area has negligible flow distribution. However, at a flow velocity of 1.9m/s, higher flow coverage is obtained with minimum stagnant zones. Thus, velocity range plays an important role in homogeneous distribution of flow inside the sensing chamber.

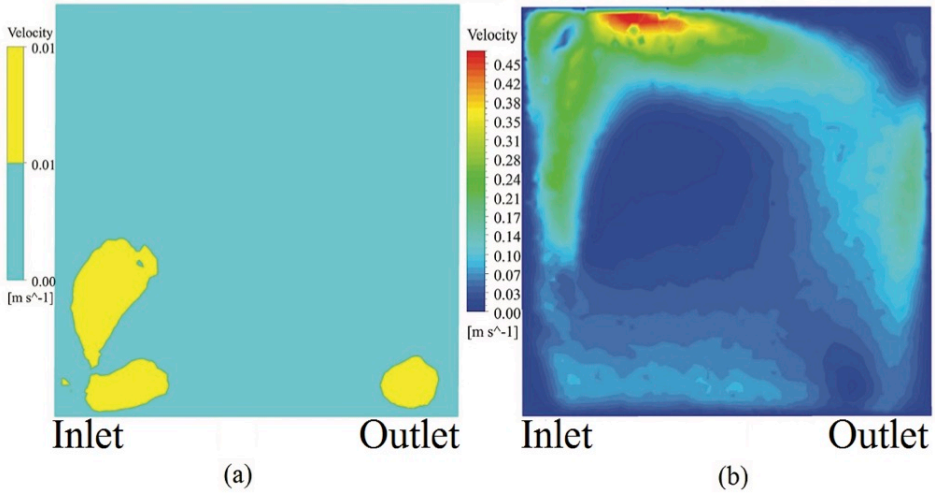

Figure 3. Velocity contours for sensor chamber 1 for flow velocity of 0.2 and 1.9 m/s (a) and (b).

This relation between input velocity and area coverage is further illustrated in Figure 4 for chamber models 1–3. It is clearly seen that for all three chambers the area coverage increases with flow velocity. For low velocities in the range of 0.1 to 0.3 m/s, flow is distributed to only 0.06%–36% of the area over the sensors. Hence, most of the sensors are not exposed to the odour analyte due to low velocity. As velocity increases beyond 0.7 m/s, flow coverage of more than 70% is obtained over the sensors.

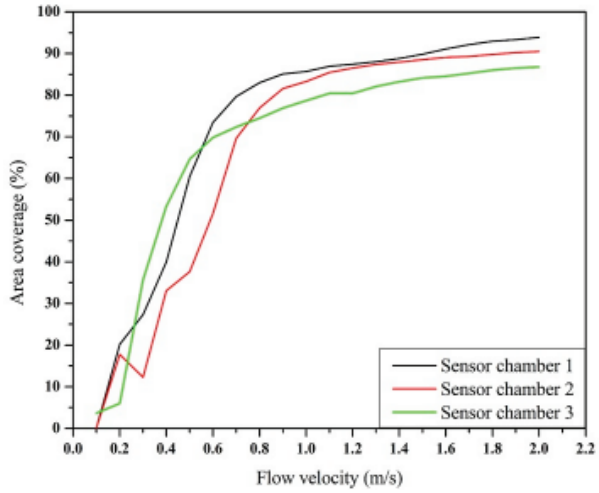

Figure 4. Area coverage graph in terms of percentage for all sensor chambers 1–3.

Velocity contours for sensor chambers 1–3 at a flow velocity of 0.7 m/s are represented in Figures 5a–5c. The dark blue region, which lies in the range 0–0.01 m/s, is considered the stagnant zone here. In these chamber models, a stagnant zone is found in the middle region. The flow distribution is maximum near the

walls as compared to other regions. The area coverage is approximately 80%, 70%, and 72% for chambers 1–3, respectively.

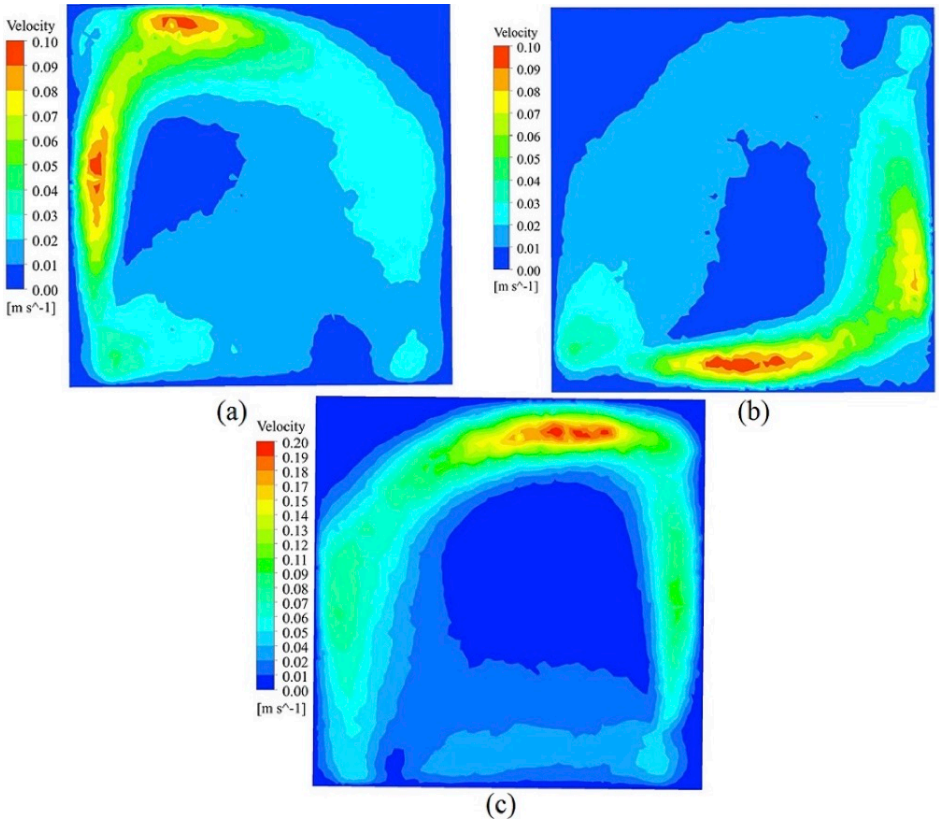

Figure 5. (a) Velocity contours for sensor chamber 1 at a flow velocity of 0.7 m/s; (b) velocity contours for sensor chamber 2 at a flow velocity of 0.7 m/s; (c) velocity contours for sensor chamber 3 at a flow velocity of 0.7 m/s.

A graphical representation of mass fraction for the flow velocities of 0.2, 0.7, and 1.2 m/s is demonstrated in Figure 6. The sensors do not receive an equal amount of mass fraction at a flow velocity of 0.2 m/s for chamber models 1–3. At 0.7 m/s, chamber 3 achieves a high mass fraction and chamber 2 obtains a low mass fraction compared to the other chambers. However, it is clearly observed that for all three chambers mass fraction increases with velocity. It is to be noted that for higher flow velocity maximum mass distribution is achieved over the sensors. Chamber 3 shows better performance compared to chambers 1 and 2. Hence, inlet and outlet positions also influence the performance of the sensor chamber [15].

Furthermore, to show the applicability for real-time analysis ethanol is used as an odour to analyse the mass fraction behaviour in the optimised sensor chamber, which is based on inlet and outlet position. The mass fraction contours at a flow velocity of 0.7 m/s for chamber 3 are shown in Figure 7. It is observed that mass fraction ranges from 0.52 to 0.57 in chamber 3 over the sensors.

3.2. Effect of baffle position on flow distribution

In order to enhance the flow distribution inside the sensor chamber, computational models consisting of four baffles are introduced at different positions in chamber model 4. Introduction of baffles improves the performance

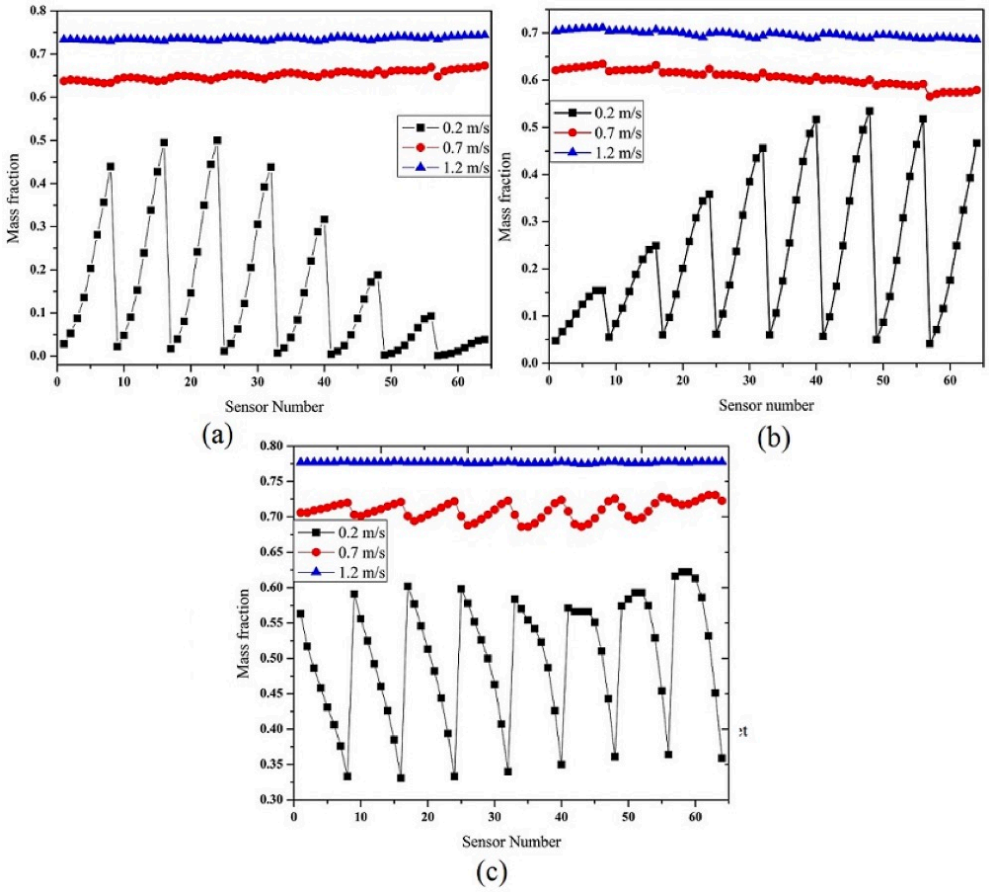

Figure 6. Mass fraction of different sensors for chambers 1 to 3 at different velocities.

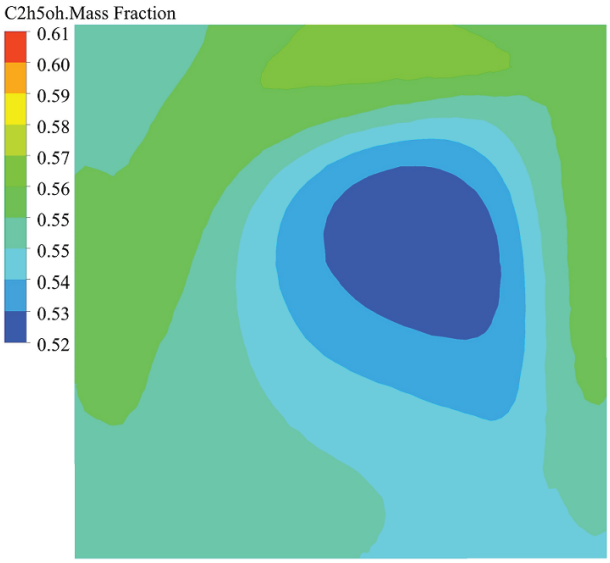

Figure 7. Mass fraction contours of sensor chamber 3 at a flow velocity of 0.7 m/s.

of the sensor chamber in terms of homogeneous airflow distribution over the sensors. Velocity contours for chambers 4–6 are demonstrated at a flow velocity of 0.7 m/s in Figure 8. It is observed that the air sample distribution over sensor chamber model 6 is 82%, while in chamber models 4 and 5 it is approximately 79% and 76%, respectively.

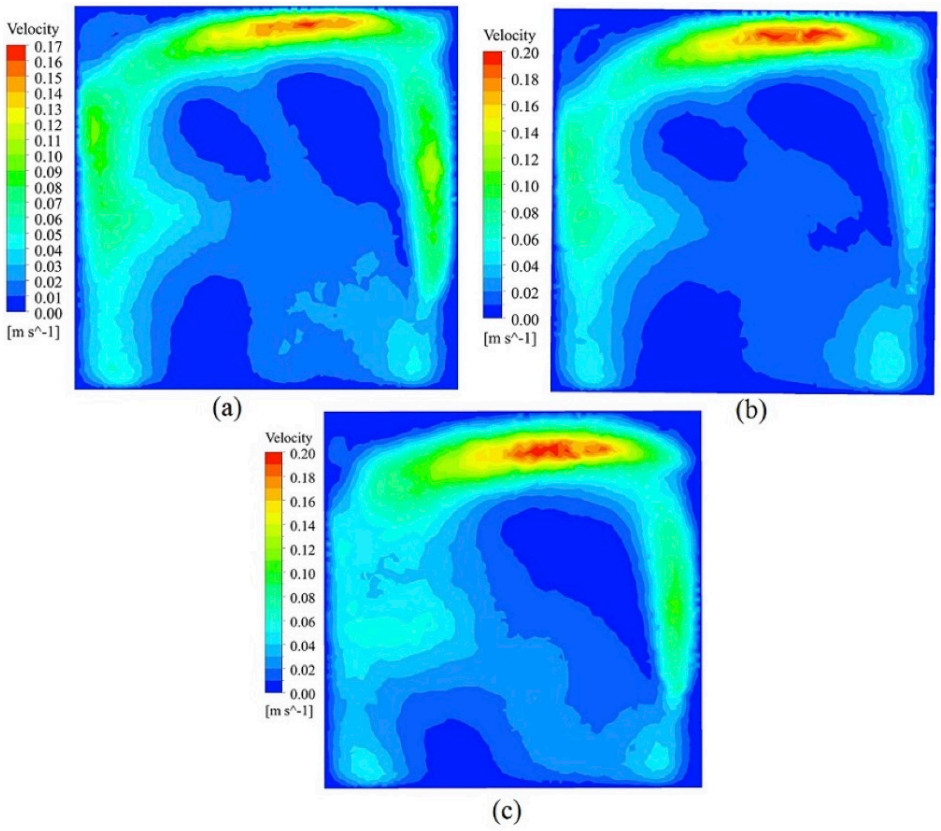

Figure 8. Velocity contours for sensor chamber 4 at a flow velocity of 0.7 m/s; (b) velocity contours for sensor chamber 5 at a flow velocity of 0.7 m/s; (c) velocity contours for sensor chamber 6 at a flow velocity of 0.7 m/s.

Baffles enhance the exposure to the odour analyte and it is observed that most of the area inside the sensor chamber is exposed to zero air. A stagnant zone is present near the inlet and middle region of the chambers and is minimum in chamber 6 as compared to the other chamber models. However, the insertion of baffles increased the airflow distribution in terms of velocity and area coverage.

The flow coverage of all the above sensor chambers is summarised for chamber models 4 to 6 in Figure 9. As velocity increases above 0.6 m/s, area coverage of more than 70% is obtained over the sensors.

A two-dimensional representation of zero air diffusion through the sensors for chamber models 4 to 6 at a flow velocity of 0.7 m/s is shown in Figure 10. Mass fraction is uniformly distributed in chambers 5 and 6 as compared to chamber 4. It is clearly observed that mass fraction ranges from 0.68 to 0.73 in chamber 4, 0.72 to 0.75 in chamber 5, and 0.71 to 0.74 in chamber 6 over the sensors. Therefore, it can be inferred that sensor chambers 5 and 6 give optimum performance in terms of a maximum mass fraction over the sensors. Hence, it can be concluded that the insertion and position of baffles ensure homogeneous flow and minimise the stagnant zone.

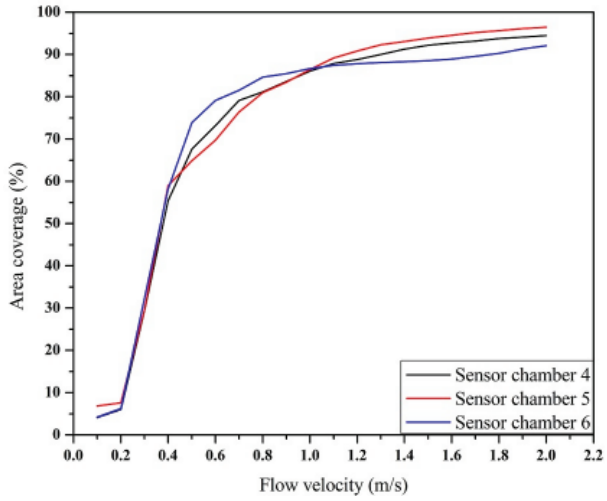

Figure 9. Area coverage graph in terms of percentage for all sensor chambers 4, 5, and 6.

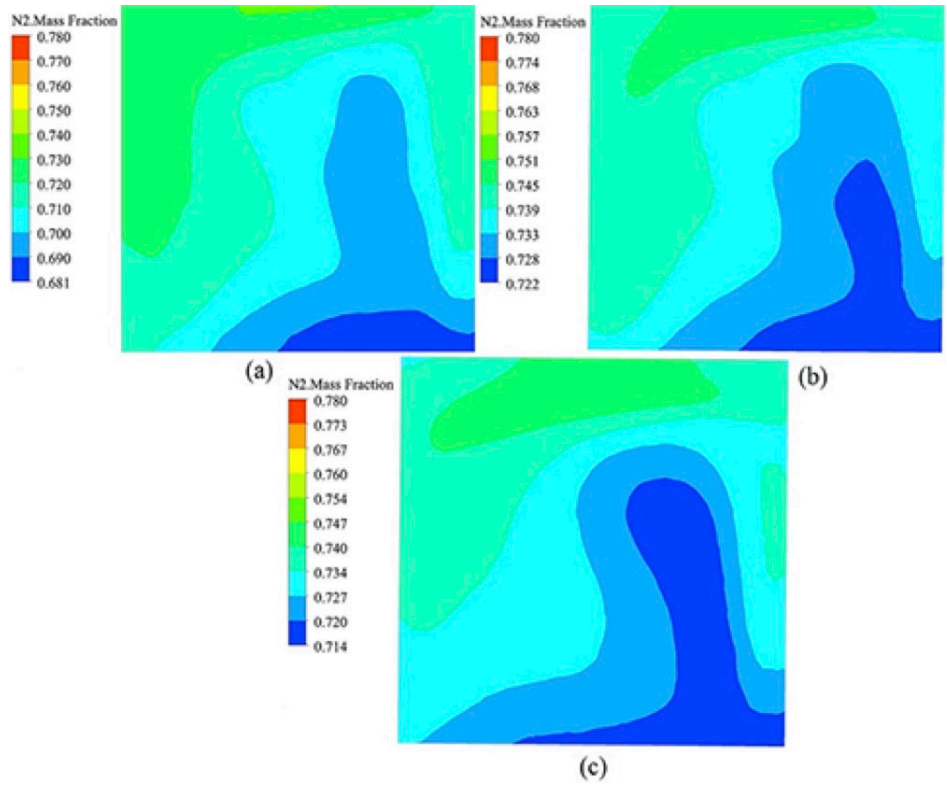

Figure 10. Mass fraction contours at a flow velocity of 0.7 m/s: (a) sensor chamber 4; (b) sensor chamber 5; (c) sensor chamber 6.

In addition, a two-dimensional contour representation of ethanol diffusion over the sensors for chamber designs 5 and 6 at a flow velocity of 0.7 m/s is shown in Figure 11. Uniformly distributed mass fraction is achieved over the sensors for these sensor chambers.

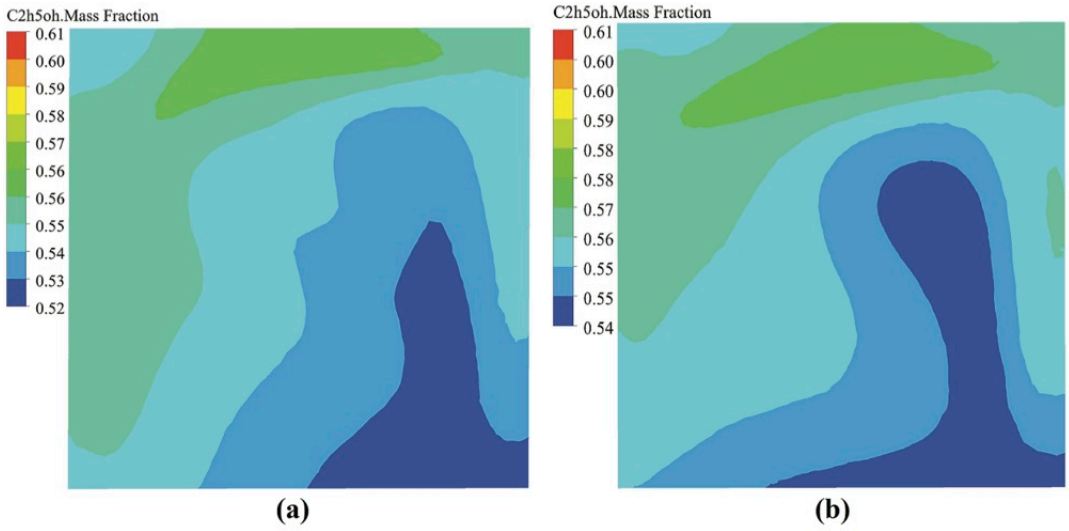

Figure 11. Mass fraction contours at a flow velocity of 0.7 m/s: (a) sensor chamber 5; (b) sensor chamber 6.

4. Conclusion

Fluid dynamics simulations were performed in six different three-dimensional sensor chambers for an electronic nose. Initially, three simple cuboids with the position and number of inlets/outlet were constructed to study the flow behaviour inside the chamber. However, a chamber with two inlets and one outlet gave better performance as compared to the other chamber. Baffles were introduced at different positions in further chamber models in order to improvise the sensor chamber design to achieve the desired performance. In this paper, the effects of baffles at different positions were examined with different flow velocity in the sensor chambers. In these sensor chambers, distribution of mass fraction over the sensor surface was optimum when baffles were included. The numerical simulations concluded that introduction of baffles at optimum position is important in the chamber in order to achieve homogeneous and maximum mass fraction distribution over the sensors.

Acknowledgements

The authors are thankful to the Council of Scientific & Industrial Research for funding the research. The authors are also thankful to the Director, CSIR-CSIO, for giving permission to carry out this work.

References

[1] Di Natale C, Macagnano A, Davide F, D'Amico A, Paolesse R et al. An electronic nose for food analysis. Sensors and Actuators B: Chemical 1997; 44 (1): 521-526.

[2] Dragonieri S, Annema JT, Schot R, van der Schee MP, Spanevello A et al. An electronic nose in the discrimination of patients with non-small cell lung cancer and COPD. Lung Cancer 2009; 64 (2): 166-170.

[3] Dragonieri S, Schot R, Mertens BJ, Le Cessie S, Gauw SA et al. An electronic nose in the discrimination of patients with asthma and controls. Journal of Allergy and Clinical Immunology 2007; 120 (4): 856-862.

[4] Capelli L, Sironi S, Del Rosso R. Electronic noses for environmental monitoring applications. Sensors 2014; 14 (11): 19979-20007.

[5] Afolabi AO, Afolabi TJ. Implementation of electronic nose technique in explosives detection. International Journal of Engineering and Science 2013; 2 (7): 10-17.

[6] Hatfield J, Neaves P, Hicks P, Persaud K, Travers P. Towards an integrated electronic nose using conducting polymer sensors. Sensors and Actuators B: Chemical 1994; 18 (1-3): 221-228.

[7] Berna A. Metal oxide sensors for electronic noses and their application to food analysis. Sensors 2010; 10 (4): 3882-3910.

[8] Wu TZ. A piezoelectric biosensor as an olfactory receptor for odour detection: electronic nose. Biosensors and Bioelectronics 1999; 14 (1): 9-18.

[9] Zhang X, Zhang M, Sun J, He C. Design of a bionic electronic nose for robot. In: Proceedings of the ISECS International Colloquium on Computing, Communication, Control, and Management; Guangzhou, China; 2008. pp. 18-23.

[10] Gardner JW, Bartlett PN. Electronic noses: principles and applications. Measurement Science and Technology 2000; 11: 1087.

[11] Falcitelli M, Benassi A, Di Francesco F, Domenici C, Marano L et al. Fluid dynamic simulation of a measurement chamber for electronic noses. Sensors and Actuators B: Chemical 2002; 85 (1): 166-174.

[12] Viccione G, Spiniello D, Zarra T, Naddeo V. Fluid dynamic simulation of odour measurement chamber. Chemical Engineering Transactions 2014; 40: 109-114.

[13] Scott S, James D, Ali Z, O'Hare W. Optimising of the sensing chamber of an array of a volatile detection system. Journal of Thermal Analysis and Calorimetry 2004; 76 (2): 693-708.

[14] Viccione G, Zarrab T, Giulianib S, Naddeob V, Belgiornob V. Performance study of e-nose measurement chamber for environmental odour monitoring. Chemical Engineering 2012; 30: 109-114.

[15] Lezzi A, Beretta G, Comini E, Faglia G, Galli G et al. Influence of gaseous species transport on the response of solid state gas sensors within enclosures. Sensors and Actuators B: Chemical 2001; 78 (1): 144-150.